

Binary Neutron Stars: Equilibrium Models beyond Spatial Conformal Flatness

Kōji Uryū,¹ François Limousin,² John L. Friedman,¹ Ericourgoulhon,² and Masaru Shibata³

¹*Department of Physics, University of Wisconsin-Milwaukee, P.O. Box 413, Milwaukee, Wisconsin 53201, USA*

²*Laboratoire de l'Univers et de ses Théories, UMR 8102 du CNRS, Observatoire de Paris, F-92195 Meudon Cedex, France*

³*Department of Earth Science and Astronomy, Graduate School of Arts and Sciences, University of Tokyo, Komaba, Meguro, Tokyo 153-8902, Japan*

(Received 25 November 2005; published 27 October 2006)

Equilibria of binary neutron stars in close circular orbits are computed numerically in a waveless formulation: the full Einstein-relativistic-Euler system is solved on an initial hypersurface to obtain an asymptotically flat form of the 4-metric and an extrinsic curvature whose time derivative vanishes in a comoving frame. Two independent numerical codes are developed, and solution sequences that model inspiraling binary neutron stars during the final several orbits are successfully computed. The binding energy of the system near its final orbit deviates from earlier results of third post-Newtonian and of spatially conformally flat calculations. The new solutions may serve as initial data for merger simulations and as members of quasiequilibrium sequences to generate gravitational-wave templates, and may improve estimates of the gravitational-wave cutoff frequency set by the last inspiral orbit.

DOI: [10.1103/PhysRevLett.97.171101](https://doi.org/10.1103/PhysRevLett.97.171101)

PACS numbers: 04.25.Dm, 04.25.Nx, 04.30.Db, 04.40.Dg

Introduction.—Equilibria of close binary neutron stars in circular orbits, constructed numerically, have been studied as a model of the final several orbits of binary inspiral prior to merger (see [1] for a review). These numerical solutions have been used as initial data sets for merger simulations [2], in quasiequilibrium sequences, to estimate gravitational waveforms [3,4], and to determine the cutoff frequency of the inspiral waves [5].

To maintain equilibrium circular orbits in general relativity one must introduce an approximation that eliminates the backreaction of gravitational radiation. An ansatz of this kind is the waveless approximation proposed by Isenberg [6]. One of his proposals was to choose a conformally flat spatial geometry maximally embedded in a spacetime. As a result, the gravitational field is no longer dynamical; field equations for the metric components become elliptic equations. Wilson and Mathews later rediscovered this waveless approximation and applied it to numerical computations of binary inspirals [7].

Although the Isenberg-Wilson-Mathews (IWM) formulation has been widely used for modeling binary neutron star and binary black hole inspiral in the past decade [5,7–12], the error associated with its conformally flat 3-geometry was studied only for stationary axisymmetric systems [13]. In models of binary neutron stars, the estimated error in the orbital angular velocity, Ω , is several percent [3,14], implying a comparable deviation from circular orbits [15]. New waveless formulations, incorporating a generic form of the metric, are suitable for accurate computation of binary compact objects [16,17]. In this Letter, we present the first results of numerical computations for binary neutron stars modeled in one of these formulations [17].

Formulation of the waveless spacetime.—The new formulation [17] exactly solves the Einstein-Euler system written in 3 + 1 form on a spacelike hypersurface. We

follow notation [18] used in [17]. The spacetime $\mathcal{M} = \mathbb{R} \times \Sigma$ is foliated by the family of spacelike hypersurfaces, $\Sigma_t = \{t\} \times \Sigma$. The future-pointing normal n^α to Σ_t is related to the timelike vector t^α (the tangent ∂_t to curves $t \rightarrow (t, x)$, $x \in \Sigma$) by $t^\alpha = \alpha n^\alpha + \beta^\alpha$, where α is the lapse, and where the shift β^α satisfies $\beta^\alpha n_\alpha = 0$. A spatial metric $\gamma_{ab}(t)$ defined on Σ_t is equal to the projection tensor $\gamma_{\alpha\beta} = g_{\alpha\beta} + n_\alpha n_\beta$ restricted to Σ_t . In terms of a conformal factor ψ and a conformally rescaled spatial metric $\tilde{\gamma}_{ab} = \psi^{-4} \gamma_{ab}$, the metric $g_{\alpha\beta}$ takes the form $ds^2 = -\alpha^2 dt^2 + \psi^4 \tilde{\gamma}_{ij}(dx^i + \beta^i dt)(dx^j + \beta^j dt)$, in a chart $\{t, x^i\}$. A condition to specify the conformal decomposition is $\det \tilde{\gamma}_{ab} = \det f_{ab}$, where f_{ab} is a flat metric.

In our waveless formulation, we impose, as coordinate conditions, maximal slicing ($K = 0$) and the spatially transverse condition $\overset{\circ}{D}_b \tilde{\gamma}^{ab} = 0$ (the Dirac gauge [17,19]), where $\overset{\circ}{D}_b$ is the covariant derivative with respect to the flat metric. We then restrict time-derivative terms in this gauge to guarantee that all components of the field equation are elliptic equations, and hence that all metric components, including the spatial metric, have Coulomb-type falloff [17]. While it is found to be sufficient to impose the condition $\partial_t \tilde{\gamma}^{ab} = O(r^{-3})$ to have Coulomb-type falloff in the asymptotics, we impose a stronger condition: $\partial_t \tilde{\gamma}^{ab} = 0$. For the other quantities, we impose helical symmetry: spacetime and fluid variables are dragged along by the helical vector $k^\alpha = t^\alpha + \Omega \phi^\alpha$. For example, the time derivative of extrinsic curvature K_{ab} is expressed as $\partial_t K_{ab} = -\mathcal{L}_{\Omega\phi} K_{ab}$. The resulting field equations are solved on a slice Σ_0 . The Hamiltonian constraint, momentum constraint, spatial trace, and spatial trace-free part of the Einstein equation are, respectively, regarded as elliptic equations for ψ , β^a , α , and $h_{ab} := \tilde{\gamma}_{ab} - f_{ab}$, while the extrinsic curvature, K_{ab} , for this formulation is computed

from the metric components, $K_{ab} = \frac{1}{2\alpha} \mathcal{L}_\beta \gamma_{ab} + \frac{1}{3\alpha} \gamma_{ab} D_c(\Omega \phi^c)$.

To compute the motion of binary neutron stars in circular orbits, the flow field is assumed to be stationary in the rotating frame. Since any solution to the waveless formulation satisfies all constraint equations, it is, in particular, an initial data set for the Einstein-Euler system. When one evolves such a binary neutron star solution by integrating the Einstein-Euler system, the orbits will deviate from exact circularity because of the radiation-reaction force. Instead, one can construct an artificial spacetime with circular orbits by dragging the waveless solution on Σ_0 along the vector $k^\alpha = t^\alpha + \Omega \phi^\alpha$, so that the spacetime has helical symmetry. Although the spacetime so constructed will not exactly satisfy Einstein's equation, a family of such spacetimes, associated with circular orbits of decreasing separation, will model the inspiral of a binary neutron star system during its final several orbits. Explicit forms of all equations for the fields and the matter are found in [17,19].

Numerical methods.—We have developed two independent numerical schemes to compute binary neutron star solutions. One is based on a finite difference method [10], the other one on a spectral method implemented via the C++ library, LORENE [20]. Detailed convergence tests and calibration of each method will be published separately. In this Letter, we show quantitative agreement of the two methods for h_{ab} , which is the significant and reliable calibration for the new numerical solutions.

In both methods, equations are written in Cartesian coordinate components, and they are solved numerically on spherical coordinate grids, r , θ , and ϕ . In the finite difference method, an equally spaced grid is used from the center of orbital motion to $5R_0$, where there are $n_r = 16, 24,$ and 32 grid points per R_0 ; from $5R_0$ to $10^4 R_0$ a logarithmically spaced grid has 60, 90, and 120 points (depending on the resolution). Here R_0 is the geometric radius of a neutron star along a line passing through the center of orbit to the center of a star. Accordingly, for θ and ϕ there are 32, 48, and 64 grid points each from 0 to $\pi/2$ [10]. For the spectral method, eight domains (a nucleus, six shells and a compactified domain extending up to infinity) around each star are used. In each domain, the number of collocation points is chosen to be $N_r \times N_\theta \times N_\phi = 25 \times 17 \times 16$ and $33 \times 21 \times 20$ [9].

Numerical solutions for binary neutron stars.—A model of the evolutionary path of binary inspiral is given by a sequence of equilibria along which the neutron star matter is assumed to be isentropic; and the implied fluid flow is assumed to conserve the baryon number, entropy, and vorticity of each fluid element [1,21]. In the case where the spins of component stars are negligible, the flow becomes irrotational; one can introduce the velocity potential Φ by $hu_\alpha = \nabla_\alpha \Phi$, where h is the specific enthalpy and u^α is the fluid 4-velocity. For isentropic flow, one can assume a one-parameter equation of state, $p = p(\rho)$, with ρ the

baryon mass density. The matter is then described by two independent variables, a thermodynamic variable such as p/ρ , and the velocity potential Φ . In this Letter, we assume a polytropic equation of state $p = \kappa \rho^\Gamma$ with adiabatic index $\Gamma = 2$, and we display results for equal-mass binaries with the rest mass of each star to be that of a single spherical star of compactness $(M/R)_\infty = 0.17$. (Note: the maximum compactness of a spherical star for this equation of state is $(M/R)_\infty = 0.216$. The compactness $(M/R)_\infty$ is defined as the ratio of gravitational mass to circumferential radius of an isolated spherical star with the same rest mass.)

In Fig. 1, contours of the components h_{ij} computed by the two numerical codes are shown for selected solutions. In these solutions, the separation in coordinate distance between the coordinate center of each neutron star is set to $a/R_0 = 3.5$. From these contours, one can verify qualitative agreement of the results from the two independent numerical methods. In Fig. 2, components h_{ij} along the x axis are plotted for the same solution, where the x axis passes through the centers of the neutron stars. Precision of integral quantities characterizing the solutions is shown by the finite difference (spectral) method comparisons: $\Omega M_\infty = 0.03565$ (0.03565), $M_{\text{ADM}}/M_\infty = 0.98825$ (0.98826), and $J/M_\infty^2 = 0.9212$ (0.9165).

In [17], it is shown that the ADM mass, M_{ADM} , and the asymptotic Komar mass, M_K , are equal, $M_{\text{ADM}} = M_K$, under asymptotic conditions satisfied by the solutions in the present formulation. The equality is related to a virial relation for the equilibrium,

$$\int x^i \gamma_i^\alpha \nabla_\beta T_\alpha^\beta \sqrt{-g} d^3x = 0, \quad (1)$$

that we use to evaluate the accuracy of numerical solutions. Figure 3 shows the computed value of the virial integral in Eq. (1), normalized by M_{ADM} , along the sequence. We also evaluated M_{ADM} and M_K each defined by the surface integral in the asymptotics, and confirmed that, for each model, the difference of the two masses is no larger than $|M_{\text{ADM}} - M_K|/M_{\text{ADM}} \sim 0.01\%$ for the finite difference

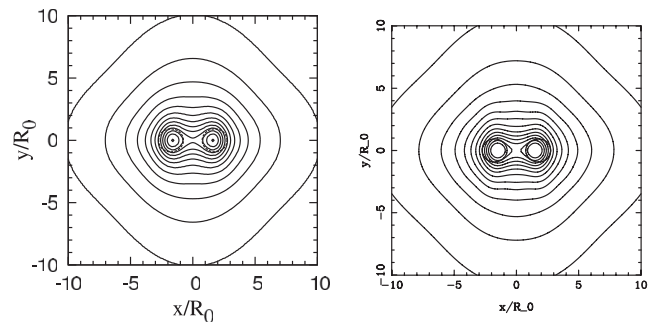


FIG. 1. Contours of $(h_{xx} - h_{yy})/2$ in the xy plane, computed by the finite difference code (left) and by the spectral code (right). The binary separation a is given by $a/R_0 = 3.5$. Contours extend from -0.014 to -0.002 with step 0.001.

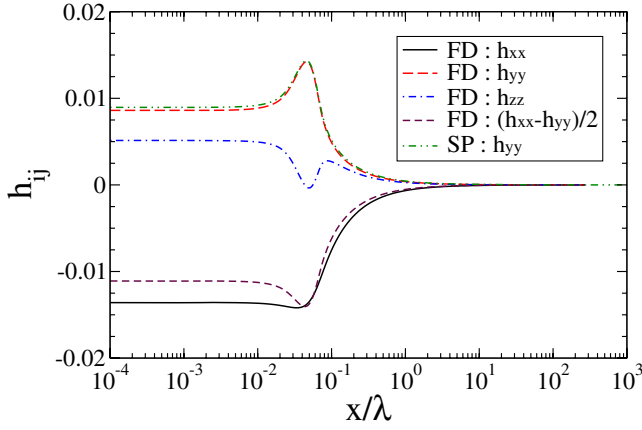


FIG. 2 (color online). Components h_{ij} along the x axis, normalized by $\lambda = \pi/\Omega$. A neutron star extends from $x/\lambda = 0.02024$ to 0.07422 . Curves labeled FD and SP display results of the finite difference and spectral codes, respectively.

method and $\sim 0.001\%$ for the spectral method; these errors are consistent with the numerical errors of the virial relation shown in Fig. 3.

In Fig. 4, the binding energy $E_b = M_{\text{ADM}} - M_\infty$ along the sequence is plotted and compared with that resulting from a third post-Newtonian (3PN) calculation [22] and IWM formulation. The waveless sequence fits the 3PN curve well at larger separation, and reaches a configuration with a cusp without any turning point in the binding energy curve, in agreement with results of the IWM formulation [9,10] (the spectral code does not yet converge for the closest orbits—largest ΩM_∞ —of Figs. 3 and 4, because it is more sensitive to tidal deformation: higher multipoles in the density of each star lead to a divergent iteration). The binding energy E_b of the waveless sequences clearly deviates from that of the 3PN and IWM sequences at the

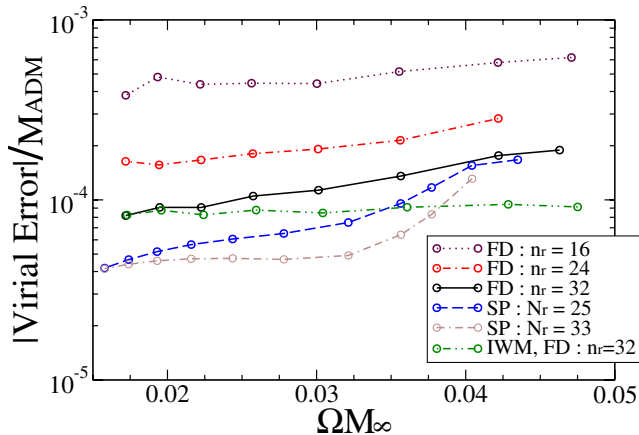


FIG. 3 (color online). Virial error vs angular velocity Ω , normalized by M_∞ , twice the gravitational mass of an isolated neutron star. Each curve labeled FD shows results of a finite difference code with a given resolution. Curves labeled SP and IWM show results of the spectral code and the spatially conformally flat approximation, respectively.

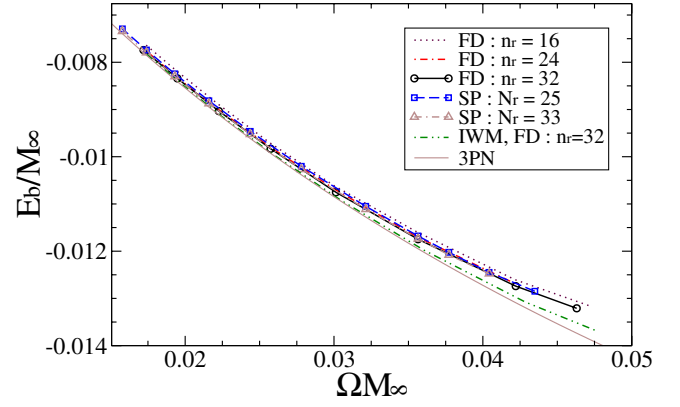


FIG. 4 (color online). Binding energy $E_b := M_{\text{ADM}} - M_\infty$ with respect to the normalized angular velocity along the sequence. Curves are labeled as in Fig. 3. The thin solid curve corresponds to the third order post-Newtonian calculation [22].

larger values of ΩM_∞ . This suggests that the 3PN and IWM formulations each overestimate the binding energy—in the 3PN case, by neglecting the tidal deformation, in the IWM formulation by neglecting the contribution from h_{ab} .

Finally, to estimate the deviation of the orbit from circularity, we evaluate the formal expression for the extrinsic curvature of a solution with exact helical symmetry (the case for which the time-evolved data have an exactly circular orbit), $\hat{K}_{ab} = \frac{1}{2\alpha} \mathcal{L}_{\beta + \Omega \phi} \gamma_{ab}$. Because $\mathcal{L}_k \hat{K}_{ab}$ vanishes for exact helical symmetry, its norm, defined on the support V of the fluid,

$$\|\mathcal{L}_k \hat{K}_{ab}\| := \left[\int_V \gamma^{ac} \gamma^{bd} \mathcal{L}_k \hat{K}_{ab} \mathcal{L}_k \hat{K}_{cd} \sqrt{\gamma} d^3x \right]^{1/2}, \quad (2)$$

is a measure of the deviation from circularity.

Figure 5 shows that, for all separations, the values of $\|\mathcal{L}_k \hat{K}_{ab}\|$ for the waveless solutions are more than an order of magnitude smaller than those of IWM solutions. The result supports the expectation that IWM data enforce

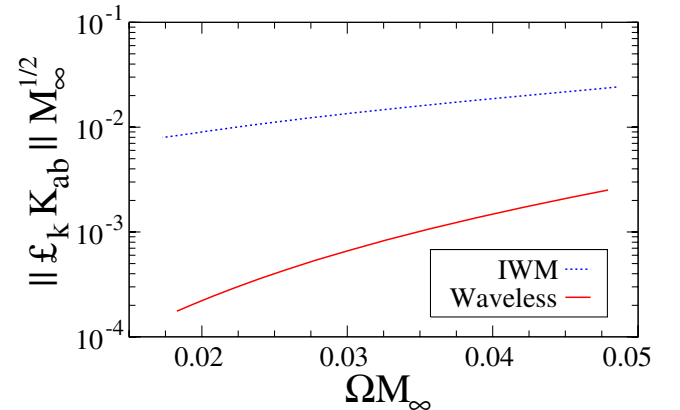


FIG. 5 (color online). Norm of Lie derivative of the extrinsic curvature along the helical vector [cf. Eq. (2)] with respect to the normalized angular velocity.

circularity with significantly less accuracy than the corresponding waveless solutions, even for larger separation. This may be important: even for a sudden turn-on of radiation reaction a post-Newtonian analysis [15] shows eccentricity $< 1.5\%$ at $\Omega M < 0.03$ for initially circular orbits, and the gravitational radiation reaction should be more gradual for our waveless data sets.

Discussion.—In second post-Newtonian theory (e.g., [14]), the correction ΔE_b to the binding energy due to the contribution of h_{ab} is of order $M_\infty h_{ab} v^a v^b$, where the magnitude of orbital velocity, v^a , may be typically $v \approx 0.34(\Omega M_\infty/0.04)^{1/3}$. Since h_{ab} is $O(v^4)$, $\Delta E_b/M_\infty = O(v^6) \sim 10^{-3}$ for $\Omega M_\infty \sim 0.04$. This agrees with the difference between the binding energies calculated by the IWM and waveless formulations in Fig. 4.

The quantity $dE_b/d\Omega$ is important for the data analysis of gravitational waves, because it determines the evolution of the wave's phase, $\Phi_{\text{GW}} = 2 \int \Omega(t) dt$. In adiabatic evolution, the time dependence of angular velocity $\Omega(t)$ is calculated from $d\Omega/dt = |(dE/dt)_{\text{GW}}|/(dE_b/d\Omega)$, where $(dE/dt)_{\text{GW}}$ is the luminosity of gravitational waves. Our present result shows that the derivative $dE_b/d\Omega$ of waveless sequences is $\sim 10\%$ – 15% larger than those of IWM and 3PN curves for $\Omega M_\infty \geq 0.035$. Since ~ 2 orbits are maintained from $\Omega M_\infty = 0.035$ to merger for the case with $(M/R)_\infty = 0.17$ [3], the error in the IWM and 3PN values of Φ_{GW} would accumulate to $\sim 50\%$ over the last ~ 2 orbits. The phase error leads to error during the final orbits before merger of the computed frequency, whose final behavior constrains the equation of state of nuclear matter [5,23]. Waveless solutions may determine phase and frequency with significantly greater accuracy—particularly if, to overcome radial-motion error, one first calibrates the frequencies of a set of quasiequilibrium sequences, using (for example) time evolutions.

Phase error may be much larger for the final orbits of binary black hole and black hole-neutron star inspirals. In these cases, ΩM_∞ in the last orbit may reach or exceed 0.1 (e.g., [11,22]). Since ΔE_b is of order $O(v^6)$, the phase error is likely to be of order unity for $\Omega M_\infty \geq 0.1$. Therefore, a template constructed from the IWM formulation may cause a systematic error in the data analysis. Our waveless approximation may improve binary black hole and black hole-neutron star solutions for this purpose.

This work was supported by Monbukagakusho Grants No. 17030004 and No. 17540232, and NSF Grants No. PHY0071044 and No. PHY0503366. K.U. thanks l'Observatoire de Paris for financial support and N. Kanda at Osaka City University.

-
- [1] T. W. Baumgarte and S. L. Shapiro, Phys. Rep. **376**, 41 (2003).
 [2] See, e.g., M. Shibata and K. Uryū, Phys. Rev. D **61**, 064001 (2000); M. Shibata, K. Taniguchi, and K. Uryū, Phys. Rev. D **68**, 084020 (2003); **71**, 084021 (2005).

- [3] M. Shibata and K. Uryū, Phys. Rev. D **64**, 104017 (2001).
 [4] M. D. Duez, T. W. Baumgarte, S. L. Shapiro, M. Shibata, and K. Uryū, Phys. Rev. D **65**, 024016 (2001).
 [5] J. A. Faber, P. Grandclément, F. A. Rasio, and K. Taniguchi, Phys. Rev. Lett. **89**, 231102 (2002); R. Oechslin, K. Uryū, G. Poghosyan, and F. K. Thielemann, Mon. Not. R. Astron. Soc. **349**, 1469 (2004); M. Bejger *et al.*, Astron. Astrophys. **431**, 297 (2005); F. Limousin, D. Gondek-Rosinska, and E.ourgoulhon Phys. Rev. D **71**, 064012 (2005).
 [6] J. Isenberg, “Waveless Approximation Theories of Gravity” (unpublished); J. Isenberg and J. Nester, in *General Relativity and Gravitation*, edited by A. Held, (Plenum, New York 1980), Vol. 1.
 [7] J. R. Wilson and G. J. Mathews, Phys. Rev. Lett. **75**, 4161 (1995); P. Marronetti, G. J. Mathews, and J. R. Wilson, Phys. Rev. D **60**, 087301 (1999).
 [8] T. W. Baumgarte, G. B. Cook, M. A. Scheel, S. L. Shapiro, and S. A. Teukolsky, Phys. Rev. D **57**, 6181 (1998); **57**, 7299 (1998).
 [9] S. Bonazzola, E.ourgoulhon, and J.-A. Marck, Phys. Rev. Lett. **82**, 892 (1999); E.ourgoulhon *et al.*, Phys. Rev. D **63**, 064029 (2001); K. Taniguchi and E.ourgoulhon, Phys. Rev. D **66**, 104019 (2002); **68**, 124025 (2003).
 [10] K. Uryū and Y. Eriguchi, Phys. Rev. D **61**, 124023 (2000); K. Uryū, M. Shibata, and Y. Eriguchi, Phys. Rev. D **62**, 104015 (2000).
 [11] E.ourgoulhon, P. Grandclément, and S. Bonazzola, Phys. Rev. D **65**, 044020 (2002); P. Grandclément, E.ourgoulhon, and S. Bonazzola, Phys. Rev. D **65**, 044021 (2002); G. B. Cook and H. P. Pfeiffer, Phys. Rev. D **70**, 104016 (2004).
 [12] J. A. Faber, P. Grandclément, and F. A. Rasio, Phys. Rev. D **69**, 124036 (2004).
 [13] G. B. Cook, S. L. Shapiro, and S. A. Teukolsky Phys. Rev. D **53**, 5533 (1996); W. Kley and G. Schäfer, Phys. Rev. D **60**, 027501 (1999); A. Garat and R. H. Price, Phys. Rev. D **61**, 124011 (2000).
 [14] H. Asada, M. Shibata, and T. Futamase, Prog. Theor. Phys. **96**, 81 (1996); H. Asada and M. Shibata, Phys. Rev. D **54**, 4944 (1996).
 [15] T. Mora and C. M. Will, Phys. Rev. D **69**, 104021 (2004); M. Miller, P. Gressman, and W.-M. Suen, Phys. Rev. D **69**, 064026 (2004); M. Miller, Phys. Rev. D **69**, 124013 (2004); P. Marronetti, M. D. Duez, S. L. Shapiro, and T. W. Baumgarte, Phys. Rev. Lett. **92**, 141101 (2004).
 [16] G. Schäfer and A. Gopakumar, Phys. Rev. D **69**, 021501(R) (2004).
 [17] M. Shibata, K. Uryū, and J. L. Friedman, Phys. Rev. D **70**, 044044 (2004); **70**, 129901(E) (2004).
 [18] Indices $a - d$ and $\alpha - \delta$ are abstract, i, j concrete.
 [19] S. Bonazzola, E.ourgoulhon, P. Grandclément, and J. Novak, Phys. Rev. D **70**, 104007 (2004).
 [20] <http://www.lorene.obspm.fr>.
 [21] C. S. Kochanek, Astrophys. J. **398**, 234 (1992); L. Bildsten and C. Cutler, Astrophys. J. **400**, 175 (1992).
 [22] L. Blanchet, Phys. Rev. D **65**, 124009 (2002).
 [23] X. Zhuge, J. M. Centrella, and S. L. W. McMillan, Phys. Rev. D **50**, 6247 (1994).